Proceedings of the CAS–CERN Accelerator School: Free Electron Lasers and Energy Recovery Linacs, Hamburg, Germany, 31 May–10 June 2016, edited by R. Bailey, CERN Yellow Reports: School Proceedings, Vol. 1/2018, CERN-2018-001-SP (CERN, Geneva, 2018)

Coherent Synchrotron Radiation and Microbunching Instability

S. Di Mitri
Elettra – Sincrotrone Trieste, Trieste, Italy

Abstract
Emission of coherent synchrotron radiation (CSR) in dipole magnets by ultra-relativistic electron beams is treated. The CSR impact on beam energy distribution and transverse emittance is discussed, and methods for minimizing emittance growth are recalled. A qualitative explanation of the contribution of CSR to the microbunching instability is given. This instability is treated in some detail in the presence of longitudinal space-charge force and magnetic bunch-length compression. Special attention is given to the aforementioned collective effects such as for the production of high peak current bunches driving free-electron lasers.

Keywords
Electron bunches; linear accelerators; electron optics; synchrotron radiation; impedance; microbunching instability.

1 Coherent synchrotron radiation

The advent of sub-picosecond-long electron beams with very high brightness in ultra-violet (UV) and X-ray free-electron lasers (FELs) driven by radio-frequency linear accelerators (RF linacs) has raised the awareness of the accelerators community to the effect of coherent synchrotron radiation (CSR) emission on the beam energy distribution and transverse emittance (primarily in the bending plane). In fact, CSR is one of the limitations associated to magnetic bunch-length compression (see previous chapter) and to transport of short bunches in multibend lines.

CSR is the low-frequency component (typically up to the THz frequency range) of electromagnetic radiation emitted by ultra-relativistic particles in dipole magnets, see Fig. 1.

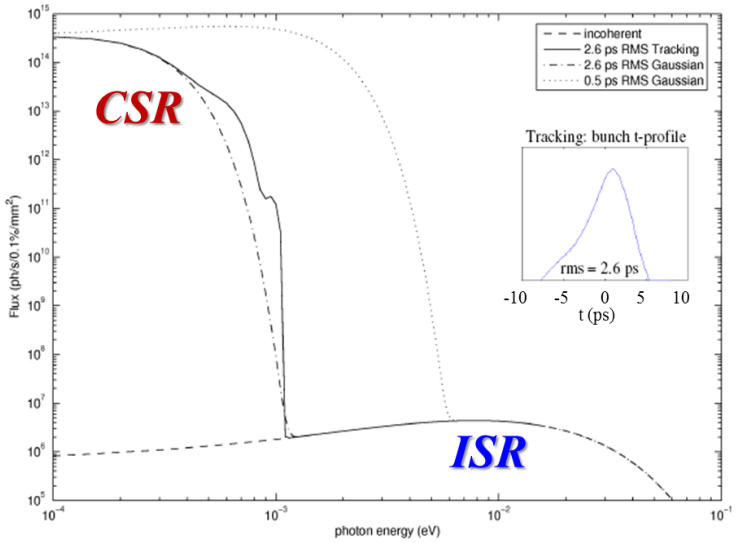

Fig. 1: Synchrotron radiation flux spectral distribution, emitted by the ~70 pC electron-bunch profile in the inset, through a dipole magnet, at the beam kinetic energy of 12.5 MeV. Courtesy of I.V. Bazarov.

https://doi.org/10.23730/CYRSP-2018-001.381

Particles are there subject to centripetal acceleration according to the Lorentz force. Radiation emitted by particles accelerated perpendicularly to their velocity is called synchrotron radiation (SR). The low-frequency part of the SR spectrum is amplified w.r.t. the high-frequency one, by the fact that electrons in the bunch are confined to a length scale of the order of, or shorter than, the radiation wavelength. As a consequence, the electric field of radiation produced by individual electrons adds in phase. This gives rise to a total radiation intensity that is proportional to the number of electrons in the bunch *squared*. In contrast, at shorter wavelengths the radiation field adds incoherently, i.e., the total intensity goes linearly with the number of beam particles. For a typical ~100 pC bunch charge, the CSR intensity is amplified by a factor ~5×10^8 w.r.t. the incoherent component.

The SR total power emitted in the fully incoherent and fully coherent regime in a dipole magnet of bending radius R is, respectively:

$$P_{\mathrm{FI}} = N \frac{e^2 c}{6\pi\varepsilon_0} \frac{\gamma^4}{R^2} \ , \qquad P_{\mathrm{FC}} = N P_{\mathrm{FI}} \ , \tag{1}$$

with N the number of particles in the bunch, γ the Lorentz factor for the beam mean energy, e the electron charge, c the light speed in vacuum and ε_0 the vacuum permittivity. The choice of beam energy and dipole radius typical of magnetic insertions in linac-driven FELs is a compromise between radiation effects and space-charge effects on the beam quality. As a result, SR is emitted in a regime of partial coherence in which the power of coherent emission is independent of beam energy (this happens for rms bunch lengths of the order of the characteristic SR wavelength $\sim R/\gamma^3$, and up to ~7 orders of magnitude longer wavelengths) [1]. In this case the total CSR power emitted by a Gaussian line-charge distribution moving along an arc is

$$P_{\mathrm{CSR}} \cong \frac{0.028c}{\varepsilon_0} \frac{Q^2}{R^{2/3}\sigma_z^{4/3}} \ . \tag{2}$$

Equation (2) shows that CSR power is highest for shortest bunches. For example, a 70 pC charge bunch with 20 μm rms bunch length emits $P_{\mathrm{CSR}}/(Nc) \cong 0.3$MeV/m energy per meter in a 2 m radius dipole. At the energy of 1 GeV, that corresponds to 0.03% loss of kinetic energy in a 1 m long magnet. This is comparable to the equivalent energy bandwidth of a UV or X-ray FEL [2]; thus, it is a significant amount of CSR power.

Owing to particles' curved path, radiation emitted by trailing particles in the bunch is allowed to catch up with leading particles within the dipole magnet (see Fig. 5 below). The primary impact of this tail–head CSR interaction [3] is a slice-by-slice change of longitudinal momentum. Such a change is in fact correlated with the z-coordinate internal to the bunch, and the z–E correlation length scale is of the order of the bunch length. Hence, particles in the same bunch slice, with a slice length much shorter than the bunch length, are subjected to the same longitudinal electric field. The change in particle energy in a dispersive region causes particles to deviate from their design trajectory. This accumulates into transverse offsets and angular divergence of bunch slices, by an amount of the order of $\Delta x \approx \eta_x \delta, \Delta x' \approx \eta'_x \delta$, where η_x, η'_x are the energy dispersion function and its longitudinal derivative, respectively, at the location of CSR emission, and δ is the CSR-induced relative energy deviation. This slice-by-slice character is illustrated in Fig. 2. Assuming typical values in magnetic compressors $\eta_x \approx 0.2\,\mathrm{m}, \eta'_x \approx 0.1\,\mathrm{rad}$ and $\delta \approx 0.03\%$, the CSR power corresponds to transverse errors of the order of $\Delta x \approx 60\,\mu\mathrm{m}, \Delta x' \approx 30\,\mu\mathrm{rad}$. These are comparable to typical unperturbed rms beam size and angular divergence. We see from such examples that it is essential to incorporate CSR in the design and optimization stage of a magnetic lattice.

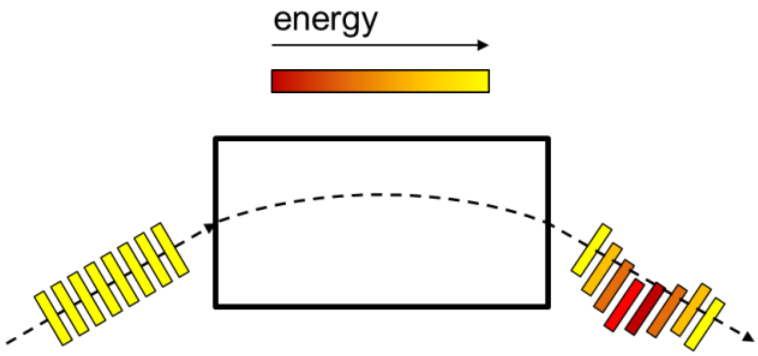

Fig. 2. Top-view representation of longitudinal bunch slices. Passing through a dipole magnet and interacting with CSR, the slices change their mean energy and energy spread. Energy change in a dispersive region causes different slices to end up at different transverse positions and angular divergences.

2 One-dimensional CSR model

The tail-to-head effect depicted in the previous section relies on the finite time that photons take to travel on a straight path from the source particle to the witness particle, in the same bunch. The CSR physics can therefore be described by taking into account the field retardation effect, i.e., the relation between the position r and time t at which a field is observed, and the retarded position r' and time t' at which this field is actually generated: $|r-r'|=c(t-t')$. The electric field E and the magnetic field B at position r and time t due to a point charge q in general motion with instantaneous velocity $\beta'=v'/c$ and acceleration $\dot{\beta}'=\dot{v}'/c$, derived from the Liénard–Wiechert retarded potentials, are [4]

$$\vec{E}(t)=\frac{q}{4\pi\varepsilon_0}\left[\frac{\vec{n}-\vec{\beta}'}{\gamma^2|\vec{r}-\vec{r}'|^2\left(1-\vec{n}\vec{\beta}'\right)^3}+\frac{\vec{n}\times\left[\left(\vec{n}-\vec{\beta}'\right)\times\dot{\vec{\beta}}'\right]}{c|\vec{r}-\vec{r}'|\left(1-\vec{n}\vec{\beta}'\right)^3}\right],$$
$$\vec{B}(t)=\frac{\vec{n}\times\vec{E}(t)}{c}, \tag{3}$$

where $n=(r-r')/|r-r'|$. The first term of the electric field in Eq. (3) is commonly named 'velocity' or 'Coulomb' term; the second one, 'acceleration' or 'radiation' term. When the distance of an observer from the emission point (say, ≥ 0.1 m or so) is much larger than the bunch length (say, ≤ 1 mm or so), the physical system of any source particle–witness particle is well aligned with the circular trajectory. For this reason, the one-dimensional (1D) approximation to the description of the CSR field can be applied when the transverse offset of particles from the reference orbit can be neglected. An estimation of the regime in which the 1D approximation applies, also named the 'Derbenev criterion', is obtained by demanding that the retarded bending angle in the 1D model is a good approximation of the actual retarded angle, as shown in Fig. 3. This brings us to the constraint $\kappa\equiv\sigma_x/\left(\sigma_z^{2/3}R^{1/3}\right)\ll 1$[3], where the symbols refer to rms transverse beam size in the bending plane, bunch length, and dipole radius. It is worth mentioning that in some cases [5, 6] the 1D model was found to reproduce well experimental evidence of transverse and longitudinal CSR effects, even if κ was approaching unity.

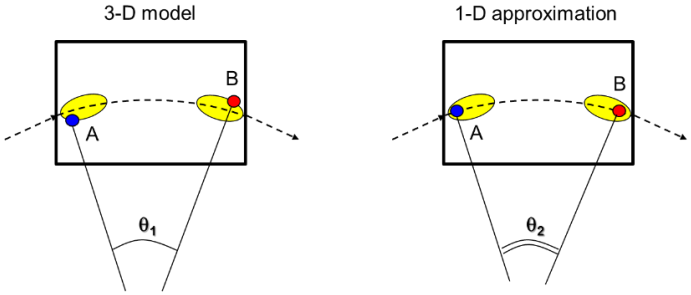

Fig. 3: CSR modelling in 1D approximation neglects the transverse offset of source and witness particles. The condition according to which $\theta_1 \cong \theta_2$ leads to the so-called Derbenev criterion (see context for details).

A rather common 1D CSR model implemented, e.g., in the `elegant` particle-tracking code [7, 8] approximates the electron bunch by a line-charge density $\lambda(z) = \frac{1}{Q}\int_{-\infty}^{\infty}\int_{-\infty}^{\infty}\rho(x,y,z)\,\mathrm{d}x\mathrm{d}y$, where $\rho(x,y,z)$ is the volume-charge density. The calculation of the retarded electromagnetic field due to $\lambda(z)$ is done on a path given by an infinitely long drift, a circular arc with radius R and angle θ, and a drift with finite length. Since any change in $\lambda(z)$ during the CSR interaction is neglected, the system is said to be in the 'frozen-beam' approximation. Namely, it is assumed that the current profile during CSR emission is the same as during CSR interaction.

The point-charge field in Eq. (3) can be used to directly calculate the electric field due to a whole charge distribution $\lambda(z)$ by a Green's function method, i.e., by considering $\lambda(z)$ as a collection of infinitesimal charges $\lambda(z)\mathrm{d}z$ and integrating (in practice, some mathematical elaborations are done in order to speed up this calculation). The result for the component of the (longitudinal) electric field tangent to the beam trajectory at the interaction point, for an observation point on the arc, turns out to be [9]

$$E_{//} = \frac{e}{24^{1/3}\pi\varepsilon_0 R^{2/3}}\left\{\frac{\left[\lambda(z-s_\mathrm{L})-\lambda(z-4s_\mathrm{L})\right]}{s_\mathrm{L}^{1/3}} + \int_{z-s_\mathrm{L}}^{z}\frac{\mathrm{d}\lambda(z')}{\mathrm{d}z'}\frac{\mathrm{d}z'}{(z-z')^{1/3}}\right\}, \tag{4}$$

where we introduced the electron–photon path-length difference or 'slippage length' $s_\mathrm{L} = R\theta - 2R\sin(\theta/2) \cong \frac{R\theta}{2\gamma^2} + \frac{R\theta^3}{24}$ over a circular arc of length $R\theta$. For beam energies of interest here, the term $\sim 1/\gamma^2$ can usually be neglected.

The term in square bracket of Eq. (4) dominates at the entrance of the dipole magnet ('entrance transient' regime of CSR emission) and finds its origin in the Coulomb term of Eq. (3). The integral dominates as θ becomes large ('steady-state' regime of CSR emission), and is mostly due to the radiation term in Eq. (3). The entrance transient effect is opposite in sign to that of the bulk contribution. It describes the physical picture in which some head particles are inside the magnet, but they do not interact with CSR because tail particles still lie outside the magnet (and therefore are not radiating yet). In `elegant`, an infinitely long drift section is always assumed at the magnet entrance. This implies that, by using the full expression of Eq. (4), the global CSR effect might be underestimated if the drift section between two consecutive dipoles is shorter than the characteristic formation length $L_\mathrm{EN} \approx \gamma R^{1/3}\sigma_z^{2/3}$ [10]. Mostly depending on beam energy, L_EN can be as long as ~0.1 m to ~10 m.

When both leading and trailing particles are inside the magnet, CSR interaction can be described in the steady-state regime. Formally, we are allowed to do this if emission happens at wavelengths comparable to bunch length, and much longer than the characteristic wavelength of incoherent synchrotron radiation (ISR), $\lambda_c \approx \frac{4\pi}{3}\left(\frac{R}{\gamma^3}\right)$. Moreover, the bunch has to be short enough to allow photons emitted by trailing particles through the dipole to overcome leading particles. In short, we assume that $R/\gamma^3 << l_b \le s_L$ [9], with l_b the characteristic bunch length. The last inequality also means that the magnet has to be longer than the characteristic distance from the magnet entrance at which transition to the steady state takes place, i.e., $l_m \ge \left(24R^2\sigma_z\right)^{1/3}$. Equivalently, the transient effect at the dipole entrance extends to approximately an angle $\theta_{tr} \approx \left(24\sigma_z/R\right)^{1/3}$, and it can be ignored w.r.t. the steady-state emission as long as the retarded bending angle $\gamma\theta >> 1$ [9]. Finally, propagation of CSR field through a drift section following the magnet enhances the global CSR effect, where the field is usually assumed to decay exponentially or so with the drift length [10].

In summary, Eq. (4) relies on the following approximations:

i) electrons are ultra-relativistic;

ii) transverse offsets of bunch particles from the reference orbit are neglected;

iii) the charge-density distribution rigidly moves along the curved path;

iv) the CSR field only influences particles ahead of emitters, i.e., radiation emitted backward is neglected;

v) the separation angle between the source particle and the witness particle is << 1;

vi) the CSR effect is assumed to be purely longitudinal, i.e., only the longitudinal component of the emitted electric field at any point tangent to the witness particle's orbit is responsible for change of its longitudinal momentum. Transverse electric field components, as well as magnetic field components, are all neglected.

As already mentioned, CSR physics relies on the CSR slippage length (it is documented that the classical expression for s_L was already known to Ipparco in ancient Greece around 100 B.C.), i.e., on the fact that photons travel straight, and doing so they catch up with electrons ahead of the source, which move on a curved path. Since angles involved are all assumed to be small, one may wonder if the angular divergence of CSR radiation is large enough to justify the tail-to-head interaction. Henceforth, we will discuss this point by limiting our attention to the steady-state regime.

It is known that most of SR is emitted in the laboratory frame in the forward direction, tangent to the source orbit, and with rms value of field intensity at angular divergence $\pm 1/(2\gamma)$, as shown in Fig. 4, left-hand plot. For example, in a case with $\gamma \ge 300$ and $\theta \le 0.1$ rad, the characteristic angle of emission of ISR would not permit any tail-to-head interaction. Instead, CSR emitted at wavelengths $\lambda >> \lambda_c$ shows an intensity field distribution with angular divergence $\sigma_\varphi \approx 0.4\left(\lambda/R\right)^{1/3}$, and approximately independent of beam energy (see Fig. 4, right-hand plot) [11]. As an example, a 10 μm long bunch bent in a 0.3 m long dipole by an angle of 0.1 rad at the energy of 300 MeV would emit ISR at $\lambda_c \approx 60$ nm with rms opening angle $1/(2\gamma) \approx 0.6$ mrad. CSR would be emitted with a characteristic opening angle from 6 mrad up to several tens of mrad. Roughly speaking, the opening angle of CSR, evaluated at wavelengths equal to or longer than the bunch length, is large enough to be comparable to the dipole bending angle, and thereby to allow photons emitted by the bunch tail to catch up with the head, inside the dipole.

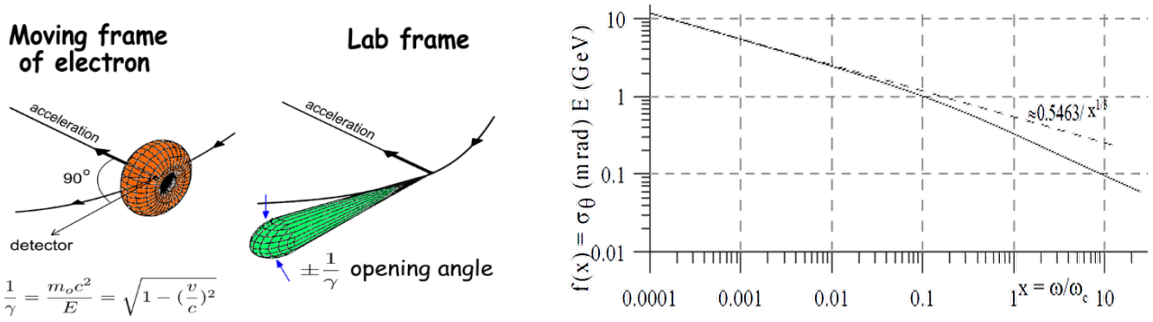

Fig. 4: Left-hand side: angular distribution of SR intensity emitted in a dipole magnet, in the moving frame of the electron and in the laboratory frame. Presented in Ref. [12]. Right-hand side: spectral dependence of SR opening angle in the bending plane. SR emitted forward at wavelengths $\lambda \le \lambda_c \approx 4\pi R/\left(3\gamma^3\right)$ shows an intensity distribution approximately Gaussian with rms width $\sigma_\varphi \cong \frac{0.6}{\gamma}\left(\frac{\lambda}{\lambda_c}\right)^{\frac{1}{3}}$. At wavelengths $\lambda >> \lambda_c$, $\sigma_\varphi \cong 0.4\left(\frac{\lambda}{R}\right)^{\frac{1}{3}}$. Published in Ref. [11].

A geometrical representation of the tail-to-head effect is given in Fig. 5, where the vectors for the electric field of Eq. (3) are shown. The source particle has a charge *q* and the witness particle is at point P. The electric field associated to the emitted radiation is orthogonal to the plane wave's direction of propagation in free space. We aim to estimate the electric field component $E_{//}$, parallel to the longitudinal velocity of the witness particle at P. We see that as long as $\theta << 1$, we can approximate the motion of *q* as if it had constant velocity, in both modulus and direction. In this case, the expression for the retarded field at P is as if it originated by a line-charge distribution at point D [4] (we are now considering the effect from a whole 1D bunch). Moreover, at large distances and high energies $\gamma >> 1$, only the 'radiation' field term in Eq. (3) contributes at P ('far-field' approximation). Hence, we can write $E\left(t;\theta << 1\right) \approx E_\perp = \lambda_z/\left(2\pi\varepsilon_0 d\right)$. By substituting the expression of *d* (see Fig. 5) and of the CSR 'overtaking length'*s* (the slippage length for an arbitrary angle θ within the dipole) into $E_\perp$, and also noticing that $E_{//} \approx E_\perp \theta$, we find $E_{//} \approx E_\perp \theta = \frac{\lambda_z \theta}{2\pi\varepsilon_0 d} \approx \frac{1}{24^{1/3}\pi\varepsilon_0}\frac{\lambda_z}{R^{2/3}s^{1/3}}$, in agreement with [3]. For a uniform line-charge distribution $\lambda_z = Q/l_b$, and for a bunch sufficiently short so that CSR emitted by the bunch tail overtakes the bunch head before the bunch leaves the magnet, we find that the single-particle energy loss per unit length is $\frac{\mathrm{d}U_e}{\mathrm{d}z} \approx -\frac{1}{24^{1/3}\pi\varepsilon_0}\frac{eQ}{R^{2/3}l_b^{4/3}}$. This result can be extended to any line-charge distribution by introducing the steady-state CSR 'wake' or Green's function [3]:

$$\frac{\mathrm{d}U_e}{\mathrm{d}z} \cong -\frac{Ne^2}{24^{1/3}\pi\varepsilon_0 R^{2/3}} \int_{z-s_L}^{z} \frac{\mathrm{d}\lambda\left(z'\right)}{\mathrm{d}z'}\frac{\mathrm{d}z'}{\left(z-z'\right)^{1/3}}. \tag{5}$$

Equation (5) is just the integral term introduced abruptly in Eq. (4). We remark that the total bunch energy loss is *N* times the single-particle one and therefore, as expected, the coherent emission shows an N^2 dependence on the total field intensity. It is also important to stress out that the CSR-induced energy loss does *not* depend on beam energy. Equation (5) suggests that the energy loss is enhanced by fast variations of $\lambda(z)$ (current spikes, fast rises of the current profile and current

modulation), so that $\mathrm{d}U_\mathrm{e}/\mathrm{d}z$ along the bunch can be monotonic or an oscillating function of z, for example, depending on the shape of the bunch current profile.

With the help of Eq. (5), we find for a Gaussian line-charge distribution:

$$\begin{aligned} U_\mathrm{e} &\cong -0.028\times Z_0 ce^2 N \frac{\theta R^{1/3}}{\sigma_z^{4/3}}, \\ \langle \delta_\mathrm{CSR} \rangle &\cong -0.35\times r_\mathrm{e} \frac{N}{\gamma} \frac{\theta R^{1/3}}{\sigma_z^{4/3}}, \\ \sigma_{\delta,\mathrm{CSR}} &\cong 0.7\times \left| \langle \delta_\mathrm{CSR} \rangle \right| \end{aligned} \tag{6}$$

for the single-particle energy loss, relative mean energy loss and rms relative energy spread, respectively. $Z_0 = 120\pi\ \Omega$ is the vacuum impedance and r_e the classical electron radius. For typical numbers in FEL linac drivers, $U_\mathrm{e} \approx 10^{-5} - 10^{-4}$ and $\langle \delta_\mathrm{CSR} \rangle \approx 10^{-4} - 10^{-3}$.

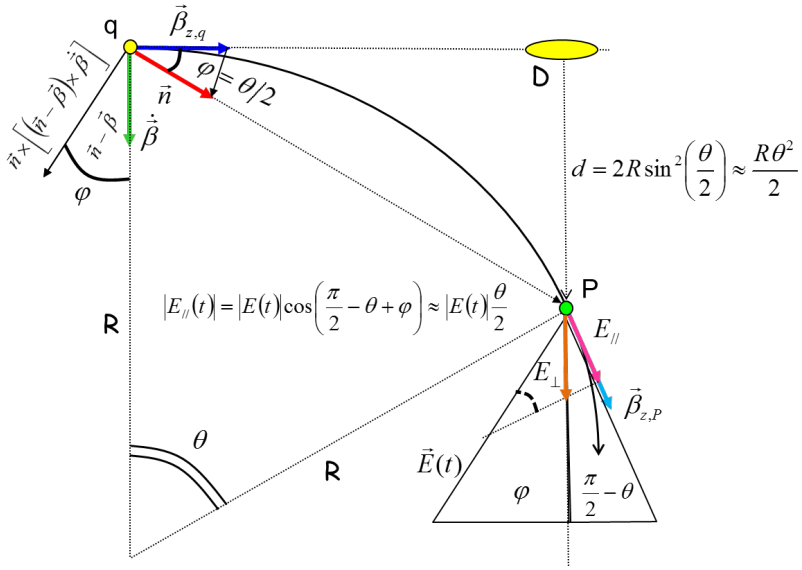

Fig. 5: Geometrical representation of CSR electric field in the 1D steady-state regime of emission in a dipole magnet. Symbols refer to Eq. (3). See context for details.

3 Transverse emittance growth

The growth of beam emittance in the bending plane is treated assuming the steady-state 1D CSR model discussed above. The transverse charge distribution in phase space (x, x') is characterized by its second-order momenta, which are associated to the so-called Twiss parameters: $\langle x_\beta^2 \rangle = \beta_x \varepsilon_x, \langle x'^2_\beta \rangle = \gamma_x \varepsilon_x, \langle x_\beta x'_\beta \rangle = -\alpha_x \varepsilon_x$; ε_x is the beam geometric emittance [13]. Particle motion is described as the linear superposition of betatron and dispersive coordinates [14]:

$$\begin{aligned} x(s) &= x_\beta(s) + R_{16}(s_0 \to s)\delta(s) \equiv x_\beta + \Delta x\ , \\ x'(s) &= x'_\beta(s) + R_{26}(s_0 \to s)\delta(s) \equiv x'_\beta + \Delta x'\ . \end{aligned} \tag{7}$$

Here δ is the relative change in longitudinal momentum due to, e.g., absorption of CSR radiation in a dipole magnet. In the presence of a *single* energy perturbation ('kick') at location s, the perturbed beam emittance becomes

$$\begin{aligned}\varepsilon_x^2 &\equiv \left\langle x_\beta^2 \right\rangle \left\langle x'^2_\beta \right\rangle - \left\langle x_\beta x'_\beta \right\rangle^2 \\ &= \varepsilon_{x,0}^2 + \varepsilon_{x,0}\left(\beta_x \left\langle \Delta x'^2 \right\rangle + 2\alpha_x \left\langle \Delta x \Delta x' \right\rangle + \gamma_x \left\langle \Delta x^2 \right\rangle\right) + \left(\left\langle \Delta x^2 \right\rangle \left\langle \Delta x'^2 \right\rangle - \left\langle \Delta x \Delta x' \right\rangle^2\right).\end{aligned} \tag{8}$$

If δ is due to *uncorrelated* events (e.g., ISR emission), the perturbed emittance results: $\varepsilon_x^2 \propto \left\langle \Delta x^2 \right\rangle_{\text{inc}} = \int_{s_0}^{s} \mathrm{d}s' R_{16}^2(s') \frac{\mathrm{d}\sigma_\delta^2(s')}{\mathrm{d}s'} \mathrm{d}s'$ (and an analogous integral of R_{26}). The integral is always positive, that is, the emittance growth is a non-reversible process. On the contrary, if δ is *correlated* with bunch length, the perturbed emittance is $\varepsilon_x^2 \propto \left\langle \Delta x^2 \right\rangle_{\text{CSR}} = \left[\int_{s_0}^{s} \mathrm{d}s' R_{16}(s') \frac{\mathrm{d}\sigma_\delta(z,s')}{\mathrm{d}s'} \mathrm{d}s'\right]^2$ (and analogously for R_{26}). In the latter case, a magnetic lattice can be designed in a way that the integral evaluated over the whole beam path is minimized or made null [15–17]. This situation applies to CSR emission, whose induced energy loss along a Gaussian bunch is shown in Fig. 6, left-hand plot.

We associate to each longitudinal bunch slice an average slice longitudinal momentum, and follow the slice centroid motion in (x, x') as predicted by Eq. (7). As a consequence of change of longitudinal momentum in a dispersive region, each slice will start moving on a different dispersive trajectory, and the beam *projected* emittance will increase according to Eq. (8) (see Fig. 6, centre plot). Moreover, since Δx and $\Delta x'$ are correlated along the bunch, we have that $\left\langle \Delta x^2 \right\rangle \left\langle \Delta x'^2 \right\rangle - \left\langle \Delta x \Delta x' \right\rangle^2 = 0$ and, given the single-kick approximation $\left\langle \Delta x^2 \right\rangle = \eta_x^2 \sigma_{\delta,\text{CSR}}^2$, $\left\langle \Delta x'^2 \right\rangle = \eta'^2_x \sigma_{\delta,\text{CSR}}^2$, with $\sigma_{\delta,\text{CSR}}$ the rms *relative* energy spread induced by CSR, we rewrite Eq. (8) as follows:

$$\varepsilon_x^2 = \varepsilon_{x,0}^2 + \varepsilon_{x,0}\left(\beta_x \left\langle \Delta x'^2 \right\rangle + 2\alpha_x \left\langle \Delta x \Delta x' \right\rangle + \gamma_x \left\langle \Delta x^2 \right\rangle\right) = \varepsilon_{x,0}^2 + \varepsilon_{x,0} H_x \sigma_{\delta,\text{CSR}}^2 \,. \tag{9}$$

Equation (9) introduces the optics function $H_x \equiv \left[\eta_x^{\,2} + \left(\beta_x \eta_x' + \alpha_x \eta_x\right)^2\right] \Big/ \beta_x$, to be evaluated at the location of the CSR kick. It suggests that CSR-induced projected emittance growth can be minimized or even cancelled through a suitable design of H-function, for any given value of $\sigma_{\delta,\text{CSR}}$. It is worth noticing that, according to this picture, the slice emittance is not affected.

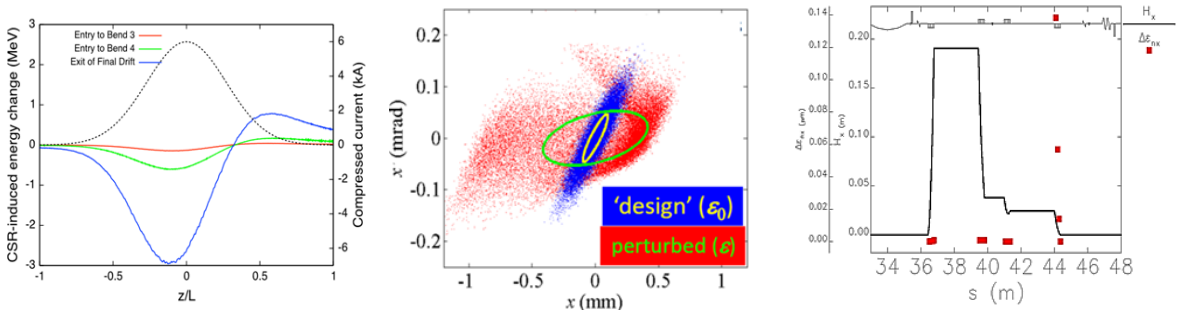

Fig. 6: (Left-hand side) CSR-induced mean slice energy difference for a Gaussian line-charge density, time compressed in a four-dipole symmetric chicane. The result is shown at the entry to third dipole (red), the entry to fourth dipole (green) and the exit of fourth dipole (blue). Published in Ref. [18]. Copyright of American Physical Society. (Middle) Charge distribution in the horizontal phase space of a beam matched to some design phase-space ellipse (blue dots), and for a beam mismatched due to CSR-induced emittance dilution (red dots). Ellipses represent second-order momenta. Courtesy of P. Emma. (Right-hand side) H-function and CSR-induced projected emittance growth along the first bunch compressor chicane of FERMI FEL. Published in Ref. [19]. Copyright of Elsevier. All plots are simulation results.

The single-kick picture in Eq. (9) usually applies to a four-dipole magnetic chicane adopted for a bunch-length compressor, and henceforth named a BC (see previous chapter). The CSR effect is strongest for a shortest bunch (see Eq. (6)) and, since the bunch approaches its final length already at the exit of the third magnet of a BC, this usually leads to a dominant CSR contribution from the fourth dipole, as shown in Fig. 6, left- and right-hand plots. Now, if the beam is forced to a horizontal waist in the second half of the chicane, and the dipoles' bending angle is small, it can be shown [19] that Eq. (9) reduces to $\varepsilon_x^2 \approx \varepsilon_{x,0}^2 + \varepsilon_{x,0}\left(\beta_x \theta^2 \sigma_{\delta,\mathrm{CSR}}^2\right)$. Thus, emittance growth can be minimized by small bending angle and small horizontal betatron function in proximity of the fourth dipole magnet [20].

The perturbed emittance at the exit of a multibend transport line, locally isochronous so that the beam has the same length at identical dipole magnets, can be expressed in the form $\varepsilon_x^2 = \varepsilon_{x,0}^2 + \varepsilon_{x,0} X\left(\alpha_x, \beta_x, \Delta\mu_x\right)_{s_\mathrm{f}} H_x\left(s_1\right)\sigma_{\delta,\mathrm{CSR}}^2$, with $H_x\left(s_1\right)$ at the location of the first CSR kick, and $X\left(\alpha_x, \beta_x, \Delta\mu_x\right)_{s_\mathrm{f}}$ is a function of Twiss parameters and relative betatron phase advance at the location of all other kicks. The energy kicks all being identical in modulus, the beam-line optics can be designed in a way that consecutive transverse kicks eventually cancel [21]. A most common and simple set-up is the one of identical Twiss parameters *and* dispersion functions at identical dipole magnets separated by π phase advance [16]. Other designs with non-symmetric optics parameters and phase advance different from π are in principle allowed. Similarly, emittance growth in a non-isochronous multibend line, such as an arc compressor, can be minimized with a proper optics design, where the 'optimal' Twiss functions now depend on the local compression factor [22, 23].

As an alternative to CSR-immune optics designs, Eq. (5) suggests that a line-charge distribution could be suitably produced at the entrance of a BC in order to generate a uniform energy loss by CSR along the bunch. In this case there would be no relative misalignment of bunch slices in phase space, and therefore no projected emittance growth [18].

4 Three-dimensional CSR model and shielding

A 3D CSR model is usually considered in numerical simulations whenever the Derbenev criterion largely fails. This may happen when a large relative energy spread or large dispersion function enlarges the beam size well above the betatron envelope, such as in the inner dipoles of a BC. Moreover, when the bunch is deflected, a longitudinal bunch slice does not stay perpendicular to the slice longitudinal momentum, but yaws with respect to it. In the former case, particles far from the beam axis, either belonging to the same slice or not, can sample a radial dependence of the CSR field. In the latter case, particles within the same slice can sample non-linearities of the longitudinal CSR field. In both cases, slice emittance growth may happen [1, 24]. Numerical predictions and experimental results suggest that these mechanisms may be playing a role already at relatively low compression factors, and affecting the slice normalized emittance at the level of ~0.1 μm rad [25, 26].

An additional complication to a CSR-dominated beam dynamics in a real lattice is provided by the shielding effect of the CSR field by the vacuum chamber [27]. In general, not all spectral components of CSR propagate in the chamber, and therefore the actual radiating energy is smaller than in a free-space environment. An analytical recipe for evaluating the shielding effect of an infinite parallel plate chamber of total height *h*, in a dipole magnet of curvature radius *R*, is [28]

$$\frac{\Delta E_{\mathrm{shield}}}{\Delta E_{\mathrm{free}}} \cong 4.2\left(\frac{n_{\mathrm{th}}}{n_{\mathrm{c}}}\right)^{\frac{5}{6}} \mathrm{e}^{-\frac{2n_{\mathrm{th}}}{n_{\mathrm{c}}}}, \quad n_{\mathrm{th}} > n_{\mathrm{c}} \ . \tag{10}$$

Here $n_{\mathrm{th}} = \sqrt{\frac{2}{3}\left(\frac{\pi R}{h}\right)^3}$ is the threshold harmonic number for propagating radiation, and $n_{\mathrm{c}} = R/\sigma_z$ is the characteristic harmonic number for a Gaussian longitudinal density distribution whose standard deviation is σ_z. The meaning of n_{c} is that the spectral component of radiation with harmonic numbers beyond it is incoherent. A more immediate although less accurate recipe for evaluating the shielding effect says that CSR emission is suppressed if $\sigma_z \geq \sqrt{\frac{h^2 w}{\pi^2 R}}$, where w is the vacuum chamber width [29].

In practice, it is difficult to shield CSR completely because, for example, a beam pipe diameter of ≤ 2 mm would be needed for ultra-relativistic sub-picosecond-long bunches. At such small gaps, resistive-wall wake field could become intolerable [30].

5 Microbunching instability

Self-developing microstructures in the longitudinal phase space of electron bunches undergoing strong compression have been observed in several high-brightness FEL linac drivers. In accordance with experimental results, computer simulations of longitudinal space charge (LSC) force (longitudinal interparticle Coulomb interaction) [31] and CSR in bunch compressors show that a so-called microbunching instability (MBI) may significantly amplify small longitudinal density and energy modulations, and hence degrade the beam quality. In its simplest picture, MBI relies on the accumulation of energy modulation induced by initial non-uniformity of the charge distribution, such as due to electron beam intrinsic shot noise or non-uniformity of the photo-injector laser pulse, and on its successive transformation to an amplified density modulation through non-isochronous ($R_{56} \neq 0$) dispersive insertions, as shown in Fig. 7 [32]. Amplified density modulations will further drive energy modulations at higher amplitudes, and thereby a positive feedback for the instability is established. The process repeats at downstream stages of acceleration and compression and, in spite of relatively high energies, the beam may eventually show strong density and energy modulations. Especially disrupting for an FEL, the beam will show large slice energy spread, at scales equal to or longer than the (shortest) modulation wavelength. The model assumes that density modulations induce energy modulations at the same wavelength(s). Moreover, the effects of LSC and of R_{56} are fully decoupled: energy modulation only happens in drift (linac) sections, while density modulation only changes through BCs. Of course, as the bunch length is compressed, the initial modulation wavelength is compressed by the same factor. At this stage of description, CSR is not needed. In fact, it amplifies the LSC-induced MBI with an analogous mechanism established in the BC.

In order to estimate the spatial scale and beam energies at which LSC and therefore MBI becomes important, we consider a two-particle 1D beam model. The beam is assumed to be ultra-relativistic, with Lorentz mean energy factor γ. One particle is at bunch centre, and it represents the whole bunch charge Q. The other particle of charge q is at the very bunch head, and the two are separated by a distance l'_{b} in the co-moving frame of the bunch. The longitudinal electric field sampled by q is $E_z' = Q/\left(4\pi\varepsilon_0 l_{\mathrm{b}}'^2\right)$. In the laboratory frame, the two particles are separated by the Lorentz-contracted length $l_{\mathrm{b}} = l'_{\mathrm{b}}/\gamma$, and the electric field sampled by q is $E_z = E_z' = Q/\left(4\pi\varepsilon_0 \gamma^2 l_{\mathrm{b}}^2\right)$. Thus, the LSC field is stronger at lower energies and at shorter scale lengths. The model also suggests that (leading) particles gain energy, while others (trailing) lose it, namely, an energy modulation builds up. The work $\Delta U = qE_z L$ done by the LSC field over a length $L \sim 10$ m becomes comparable to typical beam energies spread values at beam mean energies < 10 MeV, and at bunch length scales of the order of 1 mm. At higher beam energies, the LSC effect can only be important at wavelengths much shorter than the bunch

length, e.g., < 0.1 mm. In the following, we present a quantitative analytical treatment of MBI as induced by LSC, and compare it with other collective effects common to beam dynamics in FEL linac drivers.

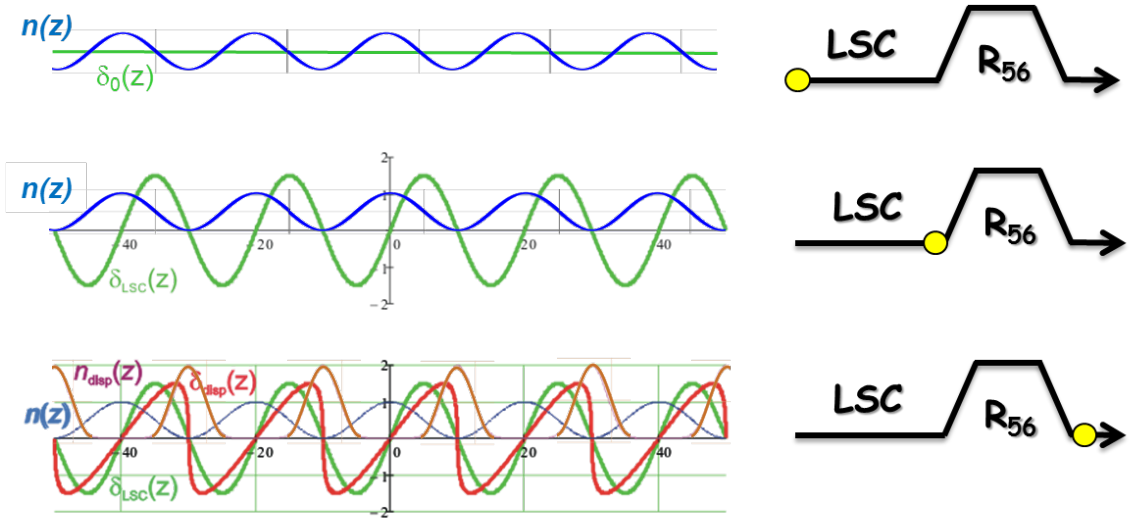

Fig. 7: Evolution (left-hand diagrams) of density (n) and energy modulation (δ) along the bunch (z), evaluated at different locations of an RF linac plus BC beam line (sketched on the right-hand side; beam is at the yellow dot). MBI is assumed to be only driven by LSC in the linac section, and by R_{56} in the BC. Upper: beam at the linac entrance has a small density modulation, and is uniform in energy. Middle: passing through the linac, the initial density modulation induces an energy modulation at the same wavelength via LSC field. Bottom: beam has passed through the BC. The longitudinal phase space is sheared due to the non-zero R_{56} in the BC ($\delta_{\rm disp}$, red curve), and the density modulation is amplified ($n_{\rm disp}$, orange curve). For a direct comparison, the initial density and energy modulations are superimposed.

6 Impedances

Accumulation of energy modulation in straight sections is driven by LSC and, at longer wavelengths, by linac geometric wake fields [30]. Since MBI is commonly studied in the frequency domain, an energy modulation at wavenumber $k = 2\pi/\lambda$ can be evaluated as the integral of the LSC impedance $Z_{\rm LSC}(k)$ over a drift length L, times the Fourier transform of the bunch peak current I [33]:

$$b(k) = \frac{1}{Nec}\int I(z)\mathrm{e}^{-\mathrm{i}kz}\mathrm{d}z \ , \qquad \Delta\gamma(k) = -\frac{4\pi I}{I_{\rm A}}b(k)\int_0^L \frac{Z(k,s)}{Z_0}\mathrm{d}s \ . \tag{11}$$

$b(k)$ is called the 'bunching factor', and its value is proportional to the density modulation amplitude *relative* to the average bunch current. For a line-charge distribution dominated by shot noise, the bunching in a bandwidth $\Delta\lambda$ can be written $b(\lambda) = \sqrt{\frac{2ec}{I\Delta\lambda}}$. The free-space LSC impedance per unit length, averaged over a Gaussian transverse distribution of rms sizes $\sigma_{x,y}$, is [34]

$$Z_{\rm LSC}(k) = \frac{\mathrm{i}Z_0}{\pi k r_{\rm b}^2}\left[1 - 2I_1(\xi)K_1(\xi)\right] , \tag{12}$$

with $\xi = kr_{\rm b}/\gamma$, I_1 and K_1 being modified Bessel functions of the first kind and $r_{\rm b} = 0.8735(\sigma_x + \sigma_y)$ is the equivalent radius of a transverse uniform distribution with area $\pi r_{\rm b}^2$ [35]. $Z_{\rm LSC}$ has a maximum for

$\xi \cong 1$. It tends to underestimate the effect of 3D fluctuations of the electric field, which happens at $\xi \geq 0.5$ [35], i.e., when the Lorentz-contracted wavelength of modulation becomes comparable to, or shorter, than the transverse beam size ('pancake-beam' scenario). In the strict 1D limit ('pencil-beam' scenario), $2I_1(\xi) \to \xi$ and, for $\xi << 1$, $I_1(\xi)K_1(\xi) \to \ln(\xi)$ [36]. Analytical approximations for Z_{LSC} in the presence of boundary conditions, for example as given by a perfectly conducting round vacuum chamber of given radius r_p, are available in the literature [37]. They rarely apply to cases of interest here because they become important at relatively long wavelengths, $\xi \leq r_b/r_p$.

In a way analogous to Eq. (12), we introduce an impedance per unit length for the CSR longitudinal electric field in a dipole of curvature radius R [38, 39], and the longitudinal geometric impedance of an RF structure of inner iris radius a [40]:

$$Z_{CSR}(k) = \frac{Z_0 k^{1/3}}{\pi R^{2/3}}(0.41 + i0.23) , \qquad Z_{RF}(k) \approx \frac{iZ_0}{\pi k a^2} . \tag{13}$$

The imaginary nature of an impedance implies a redistribution of the particles' longitudinal momentum inside the bunch, with no net energy loss, as contrary to a real impedance. In Eq. (13), the RF geometric impedance is associated to a 'wake function' in a periodic structure (this is proportional to a longitudinal electric field in the time domain) $w_{RF}(s) = \frac{Z_0 c}{\pi a^2}\exp\left(-\sqrt{s/s_0}\right)$, with $s_0 \approx 1$ mm [30], and we considered the impedance behaviour at high frequencies. Figure 8 shows the spectral domain of each of the aforementioned impedances. The typical band of interest for the MBI is at initial wavelengths in the range 1–100 μm, which, after a compression factor in the range 10–100, fit characteristic scale lengths of UV and X-ray FEL dynamics, such as FEL co-operation length and undulator slippage length [2].

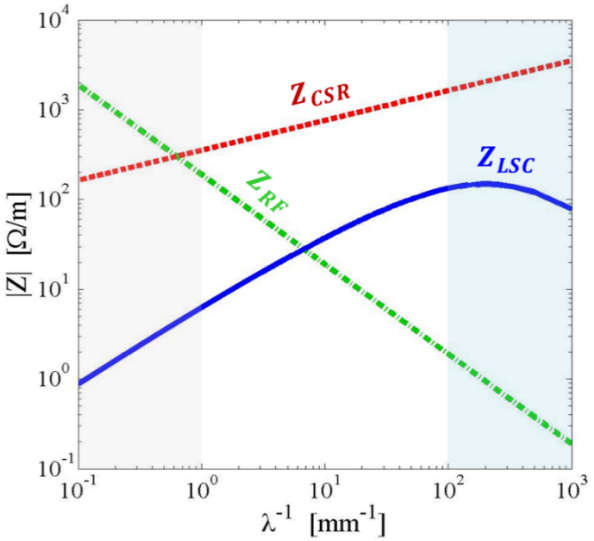

Fig. 8: Spectral behaviour of the modulus of RF, CSR and LSC impedance per unit length, see Eqs. (12) and (13). Z_{RF} is for an iris radius a = 10 mm. Z_{CSR} is calculated for R = 5 m. Z_{LSC} is calculated for a beam energy of 300 MeV and r_b = 400 μm. The shadow area on the left-hand side covers characteristic lengths of uncompressed electron bunches. The shadow area on the right-hand side highlights the typical band of interest for the MBI (wavelengths before compression).

7 Spectral gain

Modulation wavelengths of interest for FELs are usually much shorter than the electron-bunch length ('coasting beam' approximation). Moreover, it has physical sense to require that density modulation amplitudes be much smaller than the average current ('linear regime' of the instability). When both these assumptions hold, the amplitude of the density modulation at each wavelength grows *independently*, and the strength of MBI is quantified by a spectral gain $G\left(k_\mathrm{i}\right) \approx \left| b_\mathrm{f}\left(k_\mathrm{f}\right) / b_\mathrm{i}\left(k_\mathrm{i}\right)\right| \geq 0$ [32].

We now want to estimate the MBI gain in a relatively simple system, e.g. a straight section followed by a BC. Let us assume that the instability starts from a monochromatic sinusoidal modulation of the beam-current profile, $I\left(z_\mathrm{i}\right) = I_0\left[1 + A\sin\left(k_\mathrm{i} z_\mathrm{i}\right)\right]$, with A the relative modulation amplitude (the same logic and formalism applies to the case of initial energy modulation). According to Eq. (11), an energy modulation $\Delta\gamma\left(z_\mathrm{i}, k_\mathrm{i}\right) = 4\pi A \dfrac{\left|Z_\mathrm{LSC}(k_\mathrm{i})\right|}{Z_0}\dfrac{I_0}{I_\mathrm{A}} L \sin\left(k z_\mathrm{i}\right) \equiv \Delta\gamma_0 \sin\left(k z_\mathrm{i}\right)$ is accumulated over a distance L. As the beam travels with a correlated energy spread δ_c or, equivalently, a linear energy chirp h_i through the BC, the generic particle's longitudinal coordinate follows $z_\mathrm{f} = z_\mathrm{i} + R_{56}\delta_\mathrm{c} + R_{56}\,\Delta\gamma\left(z_\mathrm{i}, k_\mathrm{i}\right)/\gamma$ (see previous chapter).

We will make use of the differential form $\dfrac{\mathrm{d}z_\mathrm{f}}{\mathrm{d}z_\mathrm{i}} = 1 + h_\mathrm{i} R_{56} + R_{56}\dfrac{\Delta\gamma_0}{\gamma}\cos\left(k_\mathrm{i} z_\mathrm{i}\right)$ to find the final line-charge density: $\rho_\mathrm{f} \equiv \dfrac{\mathrm{d}N}{\mathrm{d}z_\mathrm{f}} = \dfrac{\mathrm{d}N}{\mathrm{d}z_\mathrm{i}}\dfrac{\mathrm{d}z_\mathrm{i}}{\mathrm{d}z_\mathrm{f}} \cong C\rho_\mathrm{i}\left[1 - C k_\mathrm{i} R_{56}\dfrac{\Delta\gamma_0}{\gamma}\cos\left(k_\mathrm{i} z_\mathrm{i}\right)\right]$. This expression is valid at first order in $\Delta\gamma$ and having introduced the linear compression factor $C = \left(1 + h_\mathrm{i} R_{56}\right)^{-1}$. We are now able to write down the expression for the MBI gain as a function of the initial modulation wavenumber:

$$G\left(k_i\right) \cong \left|\frac{\Delta\hat{\rho}_f / \hat{\rho}_f}{\Delta\hat{\rho}_i / \hat{\rho}_i}\right| = 4\pi C k_i \left|R_{56}\right| \frac{I_0}{I_A}\frac{\left|Z_{LSC}\left(k_i\right)\right|}{Z_0}\frac{L}{\gamma}. \tag{14}$$

Owing to the fact that any real beam has a non-zero *uncorrelated relative* energy spread $\sigma_{\delta,\mathrm{u}}$, particles belonging to the same bunch slice will travel through the BC along different path lengths because of their energy difference. The MBI gain is partially suppressed by those additional particles' longitudinal slippage. The particles' motion being uncorrelated, this process is called energy or longitudinal Landau damping, and it tends to exponentially smear energy and density modulations at relatively short wavelengths. With $\sigma_{\delta,\mathrm{u}}$ defined at the *entrance* of the BC, the MBI gain after a linac plus BC section becomes [36]:

$$G\left(k_i\right) \cong \frac{4\pi}{Z_0}\frac{I_0}{I_A} C k_i \left|R_{56}\right| \left|\int_0^L \frac{Z_{LSC}\left(k_i; s\right)}{\gamma\left(s\right)} ds\right| \exp\left[-\frac{1}{2}\left(C k_i R_{56}\sigma_{\delta,u}\right)^2\right]. \tag{15}$$

One can see that for $Z_\mathrm{LSC}(k)$ approximately constant in amplitude over a wide range of k, the gain is peaked at the wavelength that satisfies $C k_\mathrm{i} R_{56}\sigma_{\delta,\mathrm{u}} = 1$. $Z_\mathrm{LSC}(k)$ being a broadband impedance (see Fig. 8), this result is approximately true in general. Owing to the fact that the gain is exponentially suppressed by $\sigma_{\delta,\mathrm{u}}$ at short wavelengths, we find a natural cut-off of the MBI gain at $C k_\mathrm{i} R_{56}\sigma_{\delta,\mathrm{u}} \geq 1$. If the dispersive line is isochronous, and MBI is only driven by LSC in the linac, we do not expect any

gain, because particles' position inside the bunch would be the same at the entrance and at the exit of the BC.

It is worth pointing out that the gain in Eq. (15) is independent of initial modulation amplitudes. In other words, the final bunching factor is assumed to be dominated by the energy-to-density transformation that happens in the BC, and the contribution of the very initial bunching to the final bunching is neglected. This is the so-called 'high-gain' approximation. A representative LSC-induced spectral gain is shown in Fig. 9, left-hand plot, evaluated under all the approximations discussed so far.

If the MBI gain is relatively small, it may have physical sense to include the initial bunching into its expression [41]. Instead, if the linear regime of development of MBI is not satisfied (in our derivation of Eq. (14), that regime essentially corresponds to a Taylor expansion of ρ_f at first order in $\Delta\gamma$), an analytical prediction of the final gain could become a difficult task. In fact, a non-linear theory of MBI is still an open field of research [42]. For example, the linear regime may or may not apply to the case of weak compression, multistage compression schemes or to multibend lines. In a two-stage compression, the approximation of linear gain still holds through the second BC only if the bunching factor at the entrance of it is small, $\left|b_{\mathrm{f},1}\right| \ll 1$, as well as the induced energy modulation, $\left|C_1 C_2 k_\mathrm{i} R_{56,2} \Delta\gamma_2 / \gamma_\mathrm{f}\right| \ll 1$. The total gain of the beam line can in that case be estimated as the product of individual gains at the two BCs: $G_\mathrm{tot} \approx G_1 \times G_2$. Depending on beam and machine parameters, those conditions may not happen, and the total gain can largely exceed the product of individual gains. In general, the presence of numerous dipoles, such as in arcs or multibend transport lines, leads to multiple stages of amplification of the MBI, whose gain evaluation requires numerical methods.

An expression for the amplification of initial energy modulation amplitudes equivalent to Eq. (15) can be obtained as well. Here, we prefer to point out that, once the final energy modulation amplitude is computed (see Eq. (11)), an upper limit for the growth of beam *uncorrelated* energy spread due to MBI is given by the assumption that the whole modulation translates into energy spread. Such a limit is obtained by integrating the final energy modulation amplitude over all frequency components [43]:

$$\sigma^2_{\mathrm{E,MBI}} \approx \frac{\left(m_\mathrm{e} c^2\right)^2}{2\pi n_z} \int_{-\infty}^{+\infty} \mathrm{d}k_\mathrm{i} \left| G\left(k_\mathrm{i}\right)^2 \Delta\gamma_\mathrm{f}\left(k_\mathrm{i}\right)^2 \right| , \tag{16}$$

with n_z the line-charge density in m^{-1}.

The CSR contribution to MBI in compressors of FEL linac drivers is typically weaker than the one from LSC, because the effect of the latter one is summed over much longer distances. As the lattice starts being dominated by dipole magnets, however, such as in recirculating accelerators, the contribution to the gain from Z_CSR may become comparable to, if not greater than, the one from Z_LSC. In general, the CSR effect reinforces, if not drives, MBI [44]. This is because the CSR field modulates particles in energy inside dipole magnets, and the dispersion function translates energy modulations into density ones. A positive feedback for the instability, as already depicted for the LSC field, is therefore established inside the dispersive insertion [8].

At the same time, since the CSR instability couples transverse and longitudinal motion of particles, we should also consider that particles belonging to the same bunch slice but moving with different betatron amplitudes, as in a beam with non-zero horizontal geometrical emittance ε_0, will follow different path lengths. Thus, beam emittance causes some damping of the CSR-induced MBI in a way analogous to energy-Landau damping induced by $\sigma_{\delta,\mathrm{u}}$. It can be shown [19] that in order for the rms path-length difference to generate smearing of MBI at a wavenumber k, beam emittance and optics functions at the entrance of the dipole of interest must satisfy

$$k\sqrt{\varepsilon_0 H} \geq 1 \,. \tag{17}$$

The H-function can be related to R_{51} and R_{52} transport matrix terms of an arbitrary beam line. If we do so for a BC, and if some relevant CSR gain is generated in the third and fourth dipoles of it (we could expect that because the beam is shorter, and therefore the CSR field stronger, in the second half of the BC), transverse Landau damping has to be calculated by means of matrix terms that propagate particles' coordinates from the third dipole to the exit of the BC. We would therefore obtain an expression for the gain similar to that in Eq. (15), but now also dependent on Z_{CSR}, and including an additional transverse damping term describing suppression of the final bunching [45]:

$$\frac{b(k_\mathrm{i},s)}{b(k_\mathrm{i},0)} \propto \exp\left[-\frac{1}{2}\left(Ck_\mathrm{i}R_{56}\sigma_{\delta,\mathrm{u}}\right)^2\right]\exp\left\{-\frac{1}{2}C^2k_\mathrm{i}^2\left[\varepsilon_0\beta_0\left(R_{51}-\frac{\alpha_0}{\beta_0}R_{52}\right)^2-\frac{\varepsilon_0}{\beta_0}R_{52}^2\right]\right\} . \tag{18}$$

In Eq. (18), beam motion is assumed to start at coordinate $s = 0$, and the matrix terms have to be calculated at position $s > 0$; α_0, β_0 are Twiss parameters at $s = 0$. A representative 1D CSR-induced spectral gain is shown in Fig. 9 – left and right, including the effect of energy- and emittance-Landau damping. We stress that since $R_{51} = R_{52} = 0$ through a *whole* four-dipole chicane, there is no net transverse damping of MBI induced by an upstream Z_{LSC}, unless we consider a collective effect (Z_{CSR}) taking place *inside* the chicane.

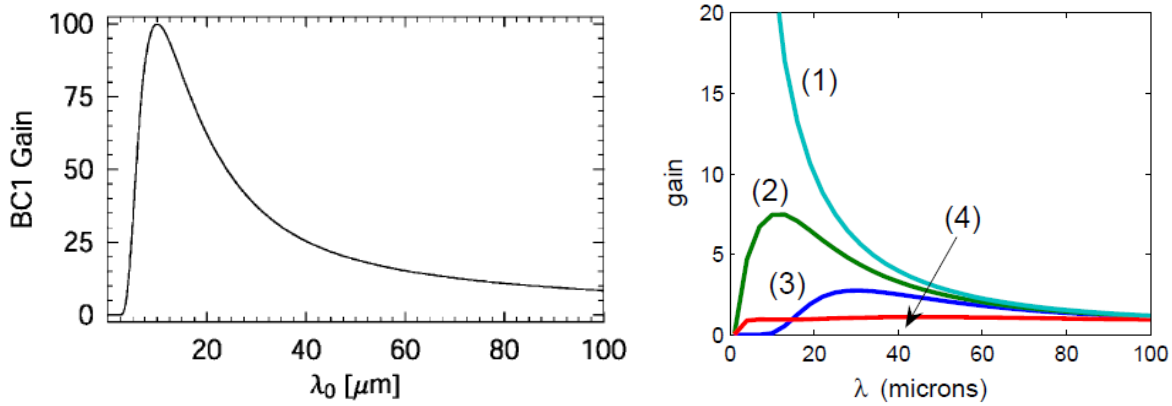

Fig. 9: (Left-hand side) MBI spectral gain induced by LSC after an RF linac section and a BC in the LCLS beam line, as a function of the initial modulation wavelength. Published in Ref. [36]. Copyright of American Physical Society. (Right-hand side) MBI spectral gain induced by CSR from a 6 kA peak current bunch in a BC at 5 GeV and R_{56} = –25 mm. Beam initial uncorrelated energy spread and normalized horizontal emittance are: (1) $\varepsilon_{n,x} = 1\,\mathrm{nm\ rad}$, $\sigma_{\delta,\mathrm{u}} = 2\times10^{-6}$; (2) $\varepsilon_{n,x} = 1\,\mu\mathrm{m\ rad}$, $\sigma_{\delta,\mathrm{u}} = 2\times10^{-6}$; (3) $\varepsilon_{n,x} = 1\,\mu\mathrm{m\ rad}$, $\sigma_{\delta,\mathrm{u}} = 2\times10^{-5}$; (4) $\varepsilon_{n,x} = 20\,\mu\mathrm{m\ rad}$, $\sigma_{\delta,\mathrm{u}} = 2\times10^{-6}$. Published in Ref. [46].

8 Laser heater

Equation (18) illustrates the two mechanisms discussed so far for suppression of MBI gain, i.e., energy- and emittance-Landau damping. Owing to the fact that, in FEL linac drivers, MBI is usually dominated by LSC, the main setting for gain suppression is to increase the beam initial uncorrelated relative energy spread. Typical energy spread values for high-brightness beams generated in RF photo-injectors are $\sigma_{\mathrm{E,u}}$ ≈ 1–3 keV [47], and the associated peak gain in long FEL drivers may be as high as 10^2–10^4. It was demonstrated in existing facilities that by increasing $\sigma_{\mathrm{E,u}}$ to 10–40 keV rms level at the beam energy of ~100 MeV, the total peak gain can be lowered by a factor of up to 10^2, and the FEL intensity is increased by a factor of up to 3 [48, 49]. Doing so, however, the final beam uncorrelated energy spread is increased

too, by approximately $\sigma_{\delta,\mathrm{f}} \approx C\sqrt{\sigma_{\delta,0}^2 + \sigma_{\delta,\mathrm{LH}}^2}$, where C is the total compression factor, $\sigma_{\delta,0}$ the natural relative energy spread at the injector exit and $\sigma_{\delta,\mathrm{LH}}$ the relative energy spread added to the beam. For an FEL, we shall still require $\sigma_{\delta,\mathrm{f}} \le 0.5\rho$ [2].

A 'laser heater' (LH) was proposed [50], and is now in operation or in design stages at several FEL facilities, in order to generate $\sigma_{\delta,\mathrm{LH}}$ in a controlled manner. Basically, a resonant interaction of electron bunches with an external infrared (IR) laser in a short undulator induces rapid energy modulation at the laser frequency. If the undulator is installed in the middle of a small chicane, the chicane geometry and the beam-line optics can be designed in a way that the IR modulation eventually washes out, and transforms into purely uncorrelated energy spread for Landau-damping purposes. Typically, the electron beam is forced to a waist in the undulator, so that the beam angular divergence is large. Then the transport through the *second* half of the chicane allows smearing of the IR modulation if $2\pi R_{52}\sigma_{x'} \ge \lambda_{\mathrm{IR}}$. Due to beam interaction with electromagnetic radiation in a dispersive section, beam emittance is also affected and its growth can be estimated at the level of $\frac{\Delta\varepsilon_x}{\varepsilon_x} \approx \frac{1}{2}\frac{\left(\eta_x\sigma_{\delta,\mathrm{LH}}\right)^2}{\beta_x\varepsilon_x}$, with optical parameters evaluated at the undulator location.

For a plane-polarized undulator with strength parameter K (see previous chapter) and length L_u, the relative energy spread induced by a LH is approximately [48]

$$\sigma_{\delta,\mathrm{LH}} \cong \frac{L_\mathrm{u}}{\sqrt{\left(\sigma_x^2+\sigma_y^2\right)}}\sqrt{\frac{P_\mathrm{L}}{2P_0}}\frac{K\left[JJ\right]}{\gamma_0^2}\,, \tag{19}$$

where σ_x, σ_y are rms electron beam sizes at the undulator, $P_0 = m_\mathrm{e}c^3/r_\mathrm{e} \cong 8.7\,\mathrm{GW}$, $L_\mathrm{u} = N_\mathrm{u}\lambda_\mathrm{u}$ is the undulator length, given by the number of undulator periods times the period length, $\left[JJ\right] = J_0\left(\varsigma\right) - J_1\left(\varsigma\right)$ are Bessel functions of argument $\varsigma = K^2/\left(4+2K^2\right)$ and P_L is the required laser peak power. Equation (19) is valid in the limit that the laser Rayleigh length is much longer than the undulator: $\pi w_0^2/\lambda_{\mathrm{IR}} >> N_\mathrm{u}\,\lambda_\mathrm{u}$, with w_0 twice the laser rms transverse size at the undulator. This ensures that the laser cross-section does not vary substantially along the undulator due to radiation diffraction.

Figure 10 shows the slice energy spread of a beam compressed in a two-BC scheme in the FERMI linac, measured at the beam energy of 1.2 GeV, as a function of the energy spread induced by a LH at 0.1 GeV (approximately 150 m upstream) [49]. For large heating levels, MBI is suppressed and the final energy spread is linearly proportional to the initial value. The constant of proportionality reflects the total compression factor $C = 7$, by virtue of the preservation of the longitudinal emittance (see previous chapter). For small heating levels, MBI 'wins' and the final energy spread is dominated by the instability gain. In this case, the final energy spread has a non-linear dependence on the initial value. In between the two regions, an optimum for the FERMI FEL is found that allows us to mitigate MBI while achieving a minimum slice energy spread at the linac end. The measurement was found to be in agreement with numerical predictions [51].

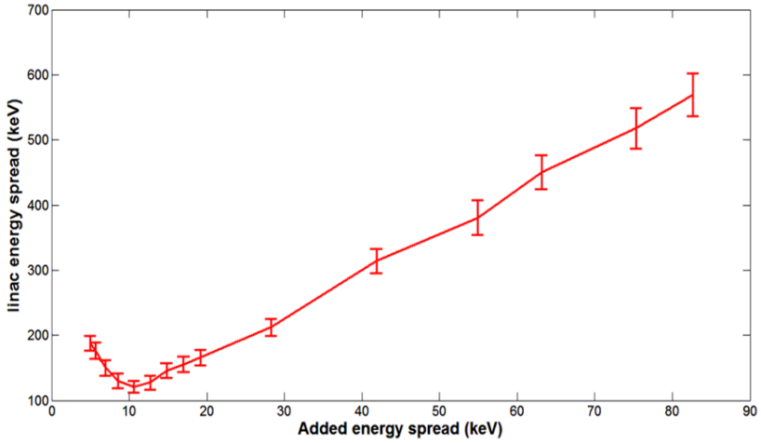

Fig. 10: Slice energy spread of a 500 pC charge bunch, compressed by a total factor of 7 in a two-BC scheme at the FERMI FEL, and measured at the energy of 1.2 GeV, as a function of the energy spread added by the LH at the energy of 0.1 GeV. Published in Ref. [49]. Copyright of American Physical Society.

9 Recent trends

Analytical modelling of MBI may become challenging when complicated beam lines are considered, and when some of the approximations depicted so far do not apply any more. Several codes are available for a numerical computation of the instability gain and of its effect on the beam energy spread, each code having its own weak and strong points. One of the major issues related to particle-in-cell codes is the one of avoiding numerical sampling noise generated by tracking (macro)particles, which are often treated in populations a few orders of magnitude smaller than the real number of beam particles. For MBI driven by shot noise, the final bunching $b_f \propto G_{tot} b_{i,sn} \propto G_{tot} \sqrt{\lambda / N}$ (see Section 6), with N the real number of electrons per modulation wavelength λ. By tracking a number of particles $N_{tr} < N$, we tend to overestimate the total gain by a factor $\sqrt{N / N_{tr}}$ [32]. Attempts to overcome this issue include filtering techniques, preparation of 'quiet' initial distributions, tracking the real number of particles, and development of algorithms intrinsically noise-free.

Present paths of research in physics of particle accelerators include practical ways to suppress the MBI, either alternative or complementary to a LH. For example, machine designs that minimize the MBI gain with a suitable compression scheme, and techniques to enhance either energy or transverse Landau damping without affecting the final beam quality. A review of such works can be found in Ref. [19]. Recently, some focus has been given to multibend lattice designs able to simultaneously minimize CSR-induced projected emittance growth and CSR-induced MBI [52].

Theoretical, numerical and experimental studies have pointed out the capability of a LH of improving the FEL intensity also as a function of transverse shaping of the LH photon pulse and, indirectly, of the electron beam energy distribution that results from the LH interaction [53]. The adoption of a LH is also opening the door to an optical shaping of the FEL pulse duration [54] and of its spectral content [55]. MBI *itself* has been used, on purpose and in a controlled manner, to enlarge the range of spectral features of a coherent light source [56, 57].

Acknowledgement

The author's present understanding of CSR effects and MBI is largely due to interactions with many colleagues, who are all acknowledged. M. Venturini and S. Spampinati are especially acknowledged for

discussions on the analytical modelling of MBI, P. Smorenburg and I. Setija for elaborations on numerical modelling and support to Figs. 2, 3 and 7 of this chapter, and S. Milton for encouragements to facing such a fascinating topic.

References

[1] M. Dohlus, Proc. Int. Committee for Future Accelerator Beam Dynamics Newsletter No. 38, Eds. I.S. Ko and W. Chou (2005).

[2] P. Schmuser, M. Dohlus and J. Rossbach, in *Ultraviolet and Soft X-ray Free-Electron Lasers*, Eds. A.-F. Chiba *et al.* (Springer, Berlin, 2008).

[3] Ya.S. Derbenev, J. Rossbach, E.L. Saldin and V.D. Shiltsev, TESLA-FEL 95-05, DESY, Hamburg, Germany (1995).

[4] Hofmann, Characteristics of synchrotron radiation, CAS Course on Synchrotron Radiation and Free-electron Lasers, Chester, UK (1989), pp. 115–141. DOI 10.5170/CERN-1990-003.115.

[5] K.L.F. Bane *et al.*, *Phys. Rev. ST Accel. Beams* **12** (2009) 030704. https://doi.org/10.1103/PhysRevSTAB.12.030704

[6] C.C. Hall *et al.*, *Phys. Rev. ST Accel. Beams* **18** (2015) 030706. https://doi.org/10.1103/PhysRevSTAB.18.030706

[7] M. Borland, APS Technical Note LS-207 (2000).

[8] M. Borland, *Phys. Rev. ST Accel. Beams* **4** (2001) 070701. https://doi.org/10.1103/PhysRevSTAB.4.070701

[9] E. Saldin *et al.*, *Nucl. Instrum. Phys. Res. A* **398** (1997) 373. https://doi.org/10.1016/S0168-9002(97)00822-X

[10] P. Emma and G. Stupakov, Proc. 8th European Accelerator Conf., WEPRI029, 2002, p. 1479.

[11] H. Wiedemann, School on Synchrotron Radiation at ICTP, Trieste, Italy (2002).

[12] L. Rivkin, CAS Course on Synchrotron Radiation Basics, Granada, Spain (2012).

[13] S.Y. Lee, *Accelerator Physics*, 2nd ed. (World Scientific, 2004), pp. 47–52 and 61–67. https://doi.org/10.1142/5761

[14] K.L. Brown, *Adv. Part. Phys.* **1** (1968) 71 and SLAC-75 Rev. 4 (1982).

[15] P. Emma and R. Brinkmann, SLAC-PUB-7554 (1997).

[16] D. Douglas, JLAB-TN-98-012 (1998).

[17] M. Venturini, *Nucl. Instrum. Methods Phys. Res. A* **794** (2015) 109. https://doi.org/10.1016/j.nima.2015.05.019

[18] C. Mitchell *et al.*, *Phys. Rev. ST Accel. Beams* **16** (2013) 060703. https://doi.org/10.1103/PhysRevSTAB.16.060703

[19] S. Di Mitri and M. Cornacchia, *Phys. Rep.* **539** (2014) 1. https://doi.org/10.1016/j.physrep.2014.01.005

[20] M. Dohlus, P. Emma and T. Limberg, in Ref. [1].

[21] S. Di Mitri, M. Cornacchia and S. Spampinati, *Phys. Rev. Lett.* **110** (2013) 014801. https://doi.org/10.1103/PhysRevLett.110.014801

[22] S. Di Mitri and M. Cornacchia, *Eur. Phys. Lett.* **109** (2015) 62002. https://doi.org/10.1209/0295-5075/109/62002

[23] S. Di Mitri, *Nucl. Instrum. Methods Phys. Res. A* **806** (2016) 184. https://doi.org/10.1016/j.nima.2015.10.015

[24] A. Novokhatski, SLAC-PUB-14893 (2012). http://slac.stanford.edu/pubs/slacpubs/14750/slac-pub-14893.pdf

[25] S. Di Mitri *et al.*, *Nucl. Instrum. Methods Phys. Res. A* **608** (2009) 19. https://doi.org/10.1016/j.nima.2009.06.028

[26] S. Bettoni *et al.*, *Phys. Rev. ST Accel. Beams* **19** (2016) 034402. https://doi.org/10.1103/PhysRevAccelBeams.19.034402

[27] V. Yakimenko, M. Fedurin, V. Litvinenko, A. Fedotov, D. Kayran and P. Muggli, *Phys. Rev. Lett.* **109** (2012) 164802. https://doi.org/10.1103/PhysRevLett.109.164802

[28] R. Li, C.L. Bohn and J.J. Bisognano, Proc. 1997 Particle Accelerator Conf., Vancouver, BC, Canada, 1997, p. 1644.

[29] R. Warnock and P. Morton, *Part. Accel.* **25** (1990) 113.

[30] K.L.F. Bane, *Int. J. Mod. Phys. A* **22** (2007) 3736. https://doi.org/10.1142/S0217751X07037391

[31] J. Rosenzweig *et al.*, DESY Report No. TESLA-FEL-96-15 (1996).

[32] E.L. Saldin, E.A. Schneidmiller and M.V. Yurkov, *Nucl. Instrum. Phys. Res. A* **490** (2002) 1. https://doi.org/10.1016/S0168-9002(02)00905-1

[33] E.L. Saldin, E.A. Schneidmiller and M.V. Yurkov, DESY Report No. TESLA-FEL-2003-02 (2003).

[34] J. Qiang *et al.*, *Phys. Rev. ST Accel. Beams* **12** (2009) 100702. https://doi.org/10.1103/PhysRevSTAB.12.100702

[35] M. Venturini, *Phys. Rev. ST Accel. Beams* **11** (2008) 034401. https://doi.org/10.1103/PhysRevSTAB.11.034401

[36] Z. Huang *et al.*, *Phys. Rev. ST Accel. Beams* **7** (2004) 074401. https://doi.org/10.1103/PhysRevSTAB.7.074401

[37] Y. Li and L. Wang, *Nucl. Instrum. Phys. Res. A* **769** (2015) 44. https://doi.org/10.1016/j.nima.2014.09.038

[38] J. Murphy, S. Krinsky, and R. Gluckstern, inProc. 1995 Particle Accelerator Conf., 1995, p. 2980.

[39] S. Heifets, S. Krinsky and G. Stupakov, *Phys. Rev. ST Accel. Beams* **5** (2002) 064401. https://doi.org/10.1103/PhysRevSTAB.5.064401

[40] R. Gluckstern, *Phys. Rev. D* **39** (1989) 2780. https://doi.org/10.1103/PhysRevD.39.2780

[41] S. Di Mitri, M. Cornacchia, S. Spampinati and S. Milton, *Phys. Rev. ST Accel. Beams* **13**(1) (2010) 010702. https://doi.org/10.1103/PhysRevSTAB.13.010702

[42] M. Venturini, *Nucl. Instrum. Methods Phys. Res. A* **599** (2009) 140. https://doi.org/10.1016/j.nima.2008.11.004

[43] D. Ratner *et al.*, *Phys. Rev. ST Accel. Beams* **18** (2015) 030704. https://doi.org/10.1103/PhysRevSTAB.18.030704

[44] M. Borland *et al.*, *Nucl. Instrum. Methods Phys. Res. A* **483** (2002) 268. https://doi.org/10.1016/S0168-9002(02)00325-X

[45] Z. Huang and K.-J. Kim, *Phys. Rev. ST Accel. Beams* **5** (2002) 074401. https://doi.org/10.1103/PhysRevSTAB.5.074401

[46] P. Piot, in Proc. 2004 Linear Accelerator Conf., WE104, Lübeck, Germany, 2004.

[47] M. Hüning and H. Schlarb, in Proc. 2003 Particle Accelerator Conf., WUPAB017, Portland, OR, USA, 2003.

[48] Z. Huang *et al.*, *Phys. Rev. ST Accel. Beams* **13** (2010) 020703. https://doi.org/10.1103/PhysRevSTAB.13.020703

[49] S. Spampinati *et al.*, *Phys. Rev. ST Accel. Beams* **17** (2014) 120705. https://doi.org/10.1103/PhysRevSTAB.17.120705

[50] E.L. Saldin, E.A. Schneidmiller andM. Yurkov, *Nucl. Instrum. Methods Phys. Res. A* **528** (2004) 355. https://doi.org/10.1016/j.nima.2004.04.067

[51] M. Venturini, *Phys. Rev. ST Accel. Beams* **10** (2007) 104401. https://doi.org/10.1103/PhysRevSTAB.10.104401

[52] C.-Y. Tsai *et al.*, in Proc. 37th Int. Free Electron Laser Conf., MOP087, Daejeon, Korea, 2015.

[53] E. Ferrari *et al.*, *Phys. Rev. Lett.* **112** (2014) 114802. https://doi.org/10.1103/PhysRevLett.112.114802

[54] Marinelli *et al.*, *Phys. Rev. Lett.* **116** (2016) 254801. https://doi.org/10.1103/PhysRevLett.116.254801

[55] E. Roussel *et al.*, *Phys. Rev. Lett.* **115** (2015) 214801. https://doi.org/10.1103/PhysRevLett.115.214801

[56] E.A. Schneidmiller and M.V. Yurkov, *Phys. Rev. ST Accel. Beams* **13** (2010) 110701. https://doi.org/10.1103/PhysRevSTAB.13.110701

[57] Marinelli *et al.*, *Phys. Rev. Lett.* **110** (2013) 264802. https://doi.org/10.1103/PhysRevLett.110.264802

Bibliography

I. S. Ko and W. Chou, Eds., ICFA Beam Dynamics Newsletter No. 38 (2005).